Published in "Inorganic Chemistry 58(9): 5646–5653, 2019"
which should be cited to refer to this work.

Anion-Induced Structural Diversity of Zn and Cd Coordination Polymers Based on Bis-9,10-(pyridine-4-yl)-anthracene, Their Luminescent Properties, and Highly Efficient Sensing of Nitro Derivatives and Herbicides

Serhii I. Vasylevskyi,*,† Dario M. Bassani,‡ and Katharina M. Fromm*,†

†University of Fribourg, Chemin du Musee 9, 1700 Fribourg, Switzerland
‡University of Bordeaux, ISM CNRS UMR 5255, 33400 Talence, France

Supporting Information

ABSTRACT: Luminescent coordination polymers (CPs) of Zn^{2+} or Cd^{2+} and bis-9,10-(pyridine-4-yl)-anthracene (**BA**) show different 1D and 2D topologies depending on the anion used in the precursor. Compounds $\{[Zn(\mu_2\text{-BA})(MeOH)_2(p\text{-Tos})_2]\}_n$ (**1**) and $\{[Zn(\mu_2\text{-BA})(MeOH)_2(CF_3CO_2)_2]\}_n$ (**2**) form linear structures and $\{BA@[Zn(\mu_2\text{-BA})(MeOH)_2(H_2O)_2](CF_3SO_3)_2\}_n$ (**3**) featuring intercalation of uncoordinated **BA** molecules into linear ribbons. Cd-based CPs $\{[Cd(\mu_2\text{-BA})_2(ClO_4)_2]\cdot n(DCM)\}_n$ (**4**) and $\{[Cd(\mu_2\text{-BA})(MeOH)_2(Dioxane)(\eta_2\text{-}SiF_6)]\cdot mDioxane\}_n$ (**5**) form porous structures with 2D lattices. All complexes exhibit strong blue emission in the solid state with average lifetimes between 8 and 13 ns. The emission of compound **4** is sensitive to the presence of nitro aromatics, simazine, and trichloroanisole (TCA) and demonstrates nonlinear Stern–Volmer quenching kinetics. Limits of detection (LOD) of 15 and 16 ppb for picric acid and TCA were achieved, respectively.

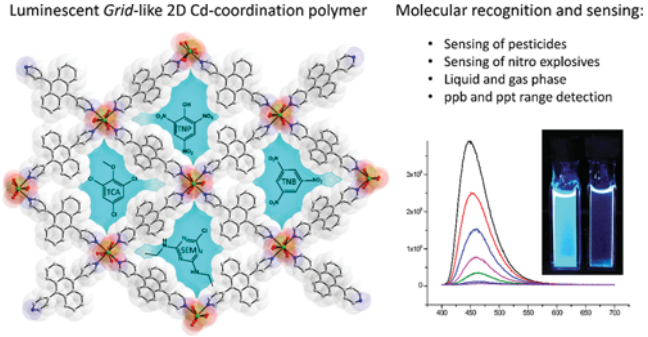

INTRODUCTION

Developing new functional coordination polymers (CPs) is particularly interesting for applications in LED,[1−5] up-conversion modules,[6−8] and for sensing traces of toxic[9−12] and explosive substances.[13] In this area, anthracene-based coordination polymers have gained interest as photoactive CPs as they exhibit luminescent behavior[14−16] that can be modulated by functional groups introduced in different positions of the anthracene chromophore.[2,17] They are generally sensitive to surrounding molecules, and this, in addition to the crystal packing arrangement, makes such anthracene-based coordination compounds attractive for application in sensing traces of nitro aromatics.[18−23] However, the design of anthracene-containing CPs in general is highly challenging, as they are very sensitive to the molecular structure of the components as well as to ancillary species such as the presence of coordinating solvent molecules and the nature of the counterions.

Early reports by the groups of Fujita[24−26] and Schröder[27,28] made evident that bis-9,10-(pyridine-4-yl)-anthracene (**BA**) forms both linear and porous coordination polymers (CPs) in the presence of various d-block metal ions. In particular, 2D supramolecular grids with dimensions of 15 × 15 Å were obtained using Cu^{2+} and Ni^{2+} salts and nitro aromatics as templates.[24] The **BA** ligand was also used as a linker to form different binuclear complexes with Cu^{2+},[28] and mixed ligand porous CPs for potential LED applications were prepared in combination with aryl dicarboxylic acids.[29] In these examples, the presence of guest molecules was shown to influence the assembly, resulting in the formation of CPs with different 1D channel topologies.[25] In other aspects of functional polymers of **BA**, Ag^{+}-CPs were shown to have a tendency for anions exchange facilitated by polar solvents.[30] Recently, a mixed ligand luminescent Zn^{2+} MOF (metal organic framework) incorporating **BA** and possessing 1D triangular channels was reported to possess high sensitivity toward hexavalent chromium species in aqueous environment.[29]

The potential applications in sensing and the structural variety of **BA**-based CPs have raised interest for the development of new luminescent anthracene-based CPs whose properties can be tuned through the nature of the metal and of the anion used for self-assembly. Herein, we compare the CPs formed by **BA** in the presence of Zn^{2+} and Cd^{2+} with different counterions. Depending on the combination of metal ion, Zn^{2+} or Cd^{2+}, 1D or 2D structures are obtained, respectively. We further show that fine-tuning of the spacing between the CP strands is possible by varying the coordinative ability of the anion. Using Cd^{2+} and coordinating perchlorate anions, a mesoporous CP architecture whose

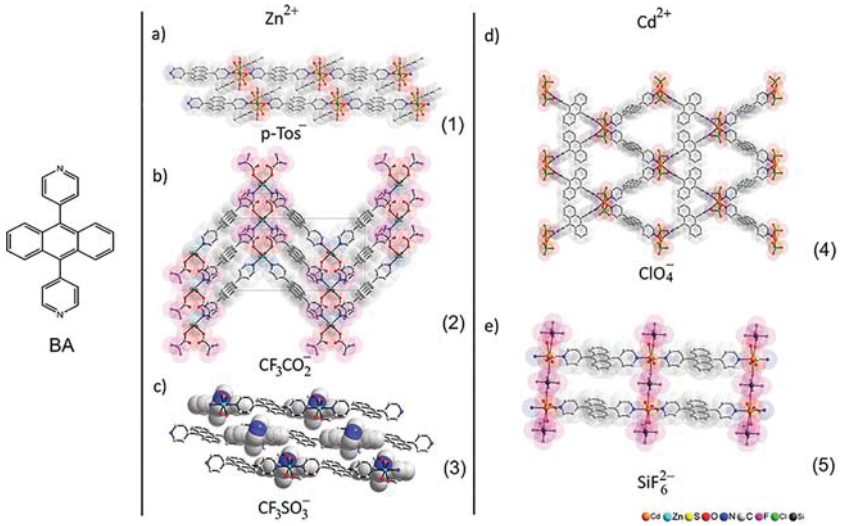

Figure 1. Formation of coordination polymers of Zn and Cd with **BA**: (a) linear 1D polymer of Zn^{2+} formed by bridging coordination of **BA** followed by self-assembly into a 2D lattice of stacked 1D polymers by H−π interactions $\{[Zn(\mu_2\text{-BA})(MeOH)_2(p\text{-Tos})_2]\}_n$ (**1**); (b) "Zig-zag" structure of the 1D coordination polymer formed with $Zn(CF_3CO_2)_2$ and **BA**, $\{[Zn(\mu_2\text{-BA})(MeOH)_2(CF_3CO_2)_2]\}_n$ (**2**); (c) 1D chains of $\{BA@[Zn(\mu_2\text{-BA})(MeOH)_2(H_2O)_2](CF_3SO_3)_2\}_n$ (**3**) with intercalation of uncoordinated **BA** (shown as space filling model); (d) 2D polymeric net of $\{[Cd(\mu_2\text{-BA})_2(ClO_4)_2]\cdot n(DCM)\}_n$ (**4**) with grid topology 4,4, formed by bridging **BA**; (e) 2D network of $\{[Cd(\mu_2\text{-BA})(MeOH)_2(Dioxane)(\eta_2\text{-}SiF_6)]\cdot mDioxane\}_n$ (**5**) by bridging coordination of **BA** and $\eta_2\text{-}SiF_6^{2-}$.

fluorescence is highly sensitive to various chloro or nitro aromatic species is obtained. This material possesses exceptional sensitivity toward nitro aromatics such as trinitrobenzene, which it can detect down to the ppt level in the vapor phase and, to the best of our knowledge, represents the first example of a CP-based fluorescent sensor for 2,4,6-trichloroanisole (TCA, detection threshold of 16 ppb).

RESULTS AND DISCUSSION

To understand the influence of anions on the self-assembly of **BA** with Zn^{2+} and Cd^{2+} metal cations, we tested various precursors of Zn^{2+} (p-Tos − tosylate; tfa − trifluoroacetate; tfl − triflate) and of isoelectronic Cd^{2+} (ClO_4^- and SiF_6^{2-}).[31] Their self-assembly in the presence of **BA** resulted in different structures of CPs being obtained from MeOH/DCM and MeOH/Dioxane solutions at room temperature (Figure 1, Table S7). In the case of $Zn(p\text{-Tos})_2$ and **BA**, self-assembly leads to the formation of a linear 1D polymer $\{[Zn(\mu_2\text{-BA})(MeOH)_2(p\text{-Tos})_2]\}_n$ (**1**) where the strands are organized through H−π interactions formed between anthracene and the tolyl-fragment of the tosylate anion (Figure 1b, and Figure S2). Under similar conditions, using $Zn(CF_3CO_2)_2$ provides 1D polymers with a "zig-zag" ribbon structure of $\{[Zn(\mu_2\text{-BA})(MeOH)_2(CF_3CO_2)_2]\}_n$ (**2**), in which the stacked anthracene moieties are now separated by the intercalation of coordinated $CF_3CO_2^-$ anions forming edge-to-face F−π interactions with the anthracene groups. Association of **BA** with $Zn(CF_3SO_3)_2$ results in a 1D polymer in which uncoordinated **BA** molecules are included in the space between the ribbons of a 1D polymer chain $\{BA@[Zn(\mu_2\text{-BA})(MeOH)_2(H_2O)_2](CF_3SO_3)_2\}_n$ (**3**) (Figure 1c and Figure S3). These guest **BA** molecules are stabilized by the formation of numerous H−π and π−π interactions between anthracene, pyridyl, and coordinated solvent molecules of H_2O and MeOH. The coordination of **BA** to Zn^{2+} ions seems to preferentially lead to assembly of 1D CPs probably due to the hard cation character of Zn^{2+} with privileged coordination of O-donors like solvents and anions in compounds **1**−**3**.[32]

In contrast to Zn^{2+}, CPs formed from Cd^{2+} salts gave 2D networks. In the case of $Cd(ClO_4)_2$ in MeOH/DCM, the Cd^{2+} ions are bridged by **BA** molecules in equatorial positions, producing a 4,4-net structure with rhombohedral pores $\{[Cd(\mu_2\text{-BA})_2(ClO_4)_2]\cdot n(DCM)\}_n$ (**4**) (Figure 1d and Figure S4) featuring distances of 11.2 × 11.2 Å in diagonal including van der Waals radii. In this case, the monovalent perchlorate anions occupy the apical/axial positions of the octahedral coordination sphere of Cd^{2+}. In contrast, the 2D CP formed from **BA** and $CdSiF_6$ $\{[Cd(\mu_2\text{-BA})(MeOH)_2(Dioxane)(\eta_2\text{-}SiF_6)]\cdot mDioxane\}_n$ (**5**) (Figure 1e and Figure S5) possesses a structure in which two of the equatorial positions at the Cd^{2+} ion are occupied by divalent, bridging SiF_6^{2-} anions and the other two by terminal methanol molecules. The **BA** ligands act as connectors between those chains. This reduces the separation between the chains, and the resulting net presents pores that are small in comparison to those in **4**, with diagonal distances of 7 × 7 Å for **5** (Figure 1e).

The luminescent properties of the Zn^{2+} and Cd^{2+} CPs **1**−**5** were investigated in solid films and as dispersions in acetonitrile (Table 1). In the solid state, **1**−**5** show similar electronic absorption spectra that are slightly different from **BA**, giving a well-resolved vibronic structure at 320−430 nm

Table 1. Solid-State Photophysical Properties of BA and CP 1−5

sample	λ_{abs} (nm)	λ_{em} (nm)	$\langle\tau\rangle^a$ (ns)	$\tau_1{}^b$ (ns)	γ^b	$\Phi_F{}^c$
BA	350−410	460	6.9			0.04
1	350−420	440	7.9	8.0	0.606	0.11
2	355−410	500	10.3	16.3	1.200	0.07
3	350−425	455, 480	13.1	12.6	2.286	0.08
4	345−405	496	14.3	14.2	0.984	0.17
5	450−400	425	10.0	13.5	1.078	0.02

[a]Intensity-averaged lifetime, λ_{ex} = 351 nm. [b]Determined according to eq 1. [c]Measured in powder samples λ_{ex} = 370 nm, (see the SI, Figures S8−S13).

characteristic of the anthracene moiety (Figure S6). However, the fluorescence emissions of the CPs differ noticeably from that of **BA**, which exhibits a structured emission with λ_{em} = 475 nm (Figure 2, Figure S7). For both **2** and **4**, a broad emission

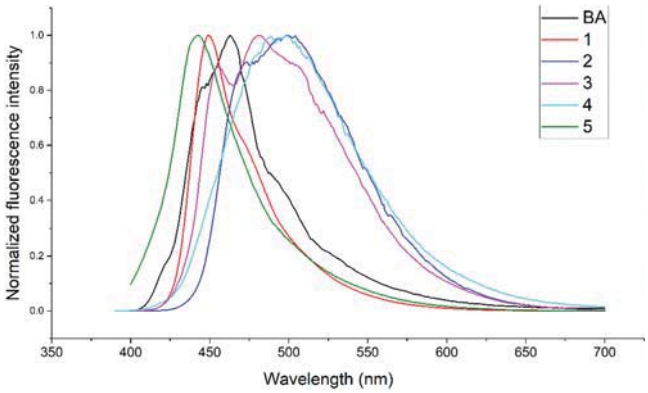

Figure 2. Solid-state emission spectra of **BA** and complexes (**1**–**5**) excited at 370 nm recorded in front-face geometry.

peak is observed at 500 nm. Close inspection of the crystal structures of **2** and **4** does not reveal the presence of proximal anthracene chromophores in a geometry suitable for the formation of excimers, and this emission is therefore assigned to the coordinated **BA** chromophores. In sharp contrast, the emission from **1** and **5** is narrow and hypsochromically shifted with respect to both coordinated and free **BA**. In the case of **5**, this is accompanied by a reduction of the fluorescence emission and is assigned to the existence of excitonic interactions between the closely packed **BA** ligands, akin to the formation of H-aggregates in the solid-state structure of **5**.[33,34] Compound **1** does not show a reduction in emission and presents a smaller hypsochromic shift than **5**, suggesting an intermediate behavior. Interestingly, the emission from **3** presents features from both coordinated and free **BA** at similar intensities, in agreement with the solid-state structure in which free **BA** molecules occupy the interstitial voids in the 1D CP. It can be concluded that, at least in this case, emission from the free **BA** ligand is competitive with energy transfer quenching to coordinated **BA** (Figure 2; **BA** and **3** emissions; black and pink traces).

The luminescence quantum yields (QYs) of the CP **1**–**5** were determined in the solid state using an integrating sphere (Horiba F-3018, λ_{ex} = 370 nm). All CPs are moderately to strongly emissive, with **4** possessing the highest photoluminescence efficiency (17%), which is much higher than the QY for the ligand alone (Table 1). Excited-state emission decays were in all cases multiexponential, and the intensity-averaged lifetimes[35] are reported in Table 1 (Figures S8–S13). In agreement with a model in which the lifetime of an emissive species is limited by energy transfer to nearby defect sites, we find that the luminescence decays of **1**–**5** can be analyzed according to eq 1[36]

$$I(t) = A + B_1 e^{[(-t/\tau_1)-2\gamma(-t/\tau_1)^{1/2}]} + B_2 e^{(-t/\tau_2)} \quad (1)$$

where $I(t)$ is the temporal dependence of the emission deconvoluted from the instrument response function, A and B are constants, τ_1 and τ_2 are the decay constants of quenched and unquenched emissive fluorophores, and γ is defined as the ratio of the quencher molar concentration to the critical molar concentration. According to this model, the lifetime of the unquenched **BA** ligand in the CPs is ca. 14 ± 2 ns with the exception of **1** in which it is somewhat shorter.

Sensing of 4 toward Pesticides and Nitro Aromatics. There are numerous examples in which the binding ability of luminescent CPs and MOFs is used to construct sensors for molecules capable of quenching luminescence through energy or electron transfer processes.[37,38] Because of their strong electron affinity, nitro aromatics represent a relatively facile class of analytes whose interest is spurred by their widespread use in explosive devices.[39] However, the monitoring of traces of pesticides and herbicides is also of fundamental importance for health and safety. To test the usefulness of **BA**-based CPs toward sensing of representative nitro aromatics and chlorinated herbicides, we selected CP **4** as it possesses the highest Φ_F and pores of sufficient size 11.2 × 11.2 Å to host potential guests (Figure S4, BET analysis is provided in the SI for **4**, Figures S65–S67 and Table S8). Complex **5** has pores that are too small to host possible analytes and exhibits a lower QY.

Target analytes include simazine (6-chloro-*N*,*N*′-diethyl-1,3,5-triazine-2,4-diamine), which is part of the widely used general-purpose atrazine family of herbicides. Although banned in Europe as a potential endocrine disruptor, it is used in the United States where it is commonly detected in the groundwater. 2,4,6-Trichloroanisole (TCA) is also of interest because it is responsible for the appearance of the corked wine fault in wines and is formed from microbial action on trichlorophenol used as a fungicide. Although not particularly toxic, human sensitivity toward trace amounts of TCA can reach 2–4 ppt.[40,41] Previous approaches to detect simazine include functionalized gold nanoparticles with porous membranes,[42] and single molecular sensors for detection of trinitrophenol (TNP).[43–45] However, poor reusability and complex synthesis of the molecular sensors and functionalization of the nanoparticles make them hardly usable in large-scale applications for the detection of nitro aromatics and herbicides. For TCA, the main challenge is the detection at levels comparable to those of humans. Recent examples include solid-state microextraction[46] and cellular biosensors with electric response.[47]

For the evaluation of the selectivity toward nitro aromatics, the following compounds were tested for comparison with previous literature reports: trinitrophenol (TNP), trinitrobenzene (TNB), 1-chloro-2,4-dinitrobenzene (CDNB), 2,4-dinitroaniline (2,4-DNA), 3,5-dinitroaniline (3,5-DNA), 3-nitrotoluene (3-NT), 2,4-dinitrotoluene (2,4-DNT), and 2,6-dinitrotoluene (2,6-DNT). Among these, only TNP, 2,6-DNT and TNB significantly quench the luminescence of **4** (see the SI, Figures S14–S42).

Static quenching of fluorescence intensity is frequently interpreted using Stern–Volmer kinetics in which the Stern–Volmer constant, $K_{SV} = KN_s$, where K and N_s are the association constant and number of binding sites, respectively. However, this model is not applicable to electron transfer quenching in solid matrices, which instead obeys an exponential relationship with respect to the quencher concentration (eq 2):[48–50]

$$\frac{I_0}{I} = e^{cv} \quad (2)$$

where I_0/I is the ratio of emission in the absence and presence of a quencher, c is the concentration of a quencher, and v is the quenching volume (defined as the volume of space

surrounding a chromophore within which a quencher will extinguish the emission of the chromophore). For these analyses, 1 mg of **4** was suspended in 2.5 mL of acetonitrile, and aliquots of the analyte solution were added. Stirring was maintained throughout the experiment to avoid precipitation of **4**. Plots of $\ln(I_0/I)$ were found to be linear in all cases, and the values of the slopes, limit of detection (LOD), and limit of quantification (LOQ) are collected in Table 2 (Figures S47–S51 and Tables S1–S6).[51] For comparison with the literature, the value of K_{SV} in the quasilinear regime at low analyte concentrations are also reported (Table S7).

Table 2. Sensing Properties of CP 4[a]

analyte	K_{SV}[b] L/mol	cv[c]	LOD nM (ppb)[d]	LOQ μM (ppb)[d]
TCA	90 200	54 300	61 (16.5)	0.28 (76)
SIM	40 200	36 000	478 (122)	3.65 (932)
TNP	139 200	66 800	54 (15.6)	0.31 (90)
TNB	36 900	33 000	1650 (448)	2.17 (590)
DNT	77 800	45 700	320 (74)	0.56 (129)

[a]In acetonitrile solution, λ_{ex} = 370 nm. [b]Determined at low analyte concentration. [c]Determined according to eq 2. [d]In ppb by weight. (Detailed calculations provided in the SI, Tables S1–S6.)

The results show that **4** possesses excellent sensitivity for both nitro aromatics as well as for TCA and simazine (see Figures 3 and 4 for TCA and TNP, and Figures S14–S42 for

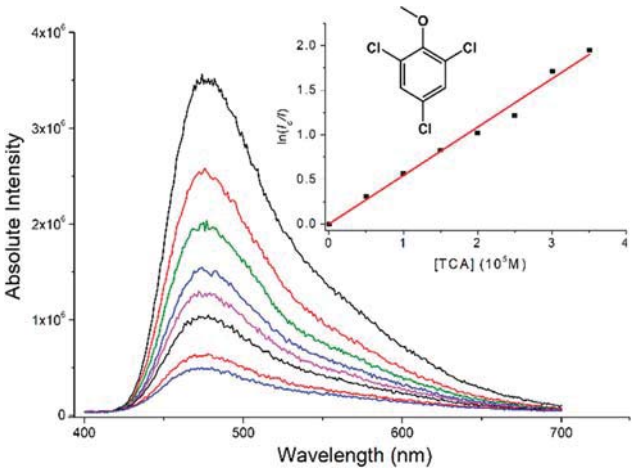

Figure 3. Fluorescence sensing of 2,4,6-trichloroanisole (TCA) by CP **4** in MeCN. Inset: plot of the quenching of **4** by TCA according to eq 2.

other analytes). To the best of our knowledge, **4** represents the first example of a fluorometric CP-based sensor for TCA. Its sensitivity toward simazine greatly surpasses that of fluoro-assays based on specifically imprinted polymers, and the LOD determined for TNP compares well with the lowest detection thresholds of 2.9 and 0.9 ppb reported to date.[52,53]

Compared to other luminescent CPs, **4** possesses the added advantage of absorbing and emitting at longer wavelengths, which lowers possible interference by other emissive species in the matrix. In the case of TNP, a bathochromic shift of the emission spectrum can be observed, indicating the presence of specific interactions between the CP and TNP (Figure 4). This is further supported by the greater response of **4** toward TNP versus TNB despite the latter's greater electron affinity.

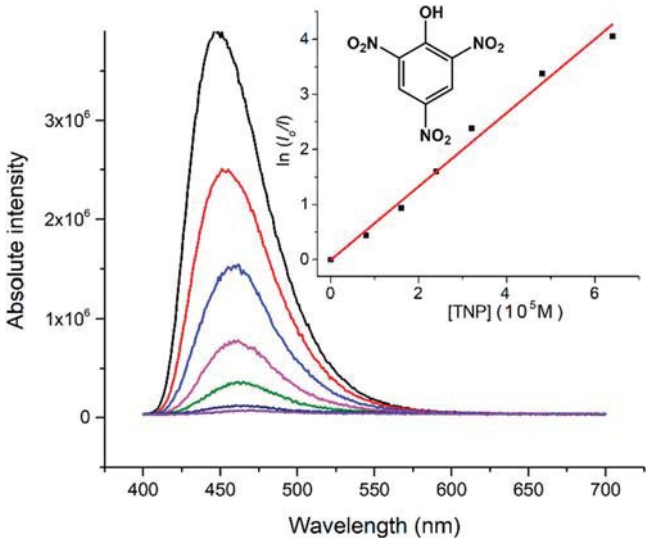

Figure 4. Fluorescence sensing of picric acid (TNP) by CP **4** in MeCN. Inset: plot of the quenching of **4** by TNP according to eq 2.

Compound **4** is stable to water and moisture, which renders it interesting for direct sensing in aqueous or gaseous environments by immobilizing it on a solid support. To test the vapor-phase sensing ability of **4** toward TCA and TNB, a dispersion of **4** in MeOH/DCM was drop-cast onto 2 × 2 cm borosilicate substrates. After evaporation, the emission from **4** was recorded using a front-face geometry. A small sample of TCA or TNB was then placed in the sealed sample chamber of the spectrofluorimeter and allowed to equilibrate over several hours during which time the emission spectrum was recorded. The results are shown in Figure 5 (Figures S43–S46), where it can be seen that a strong signal response was obtained in both cases. Both TCA and TNB possess low partial vapor pressures

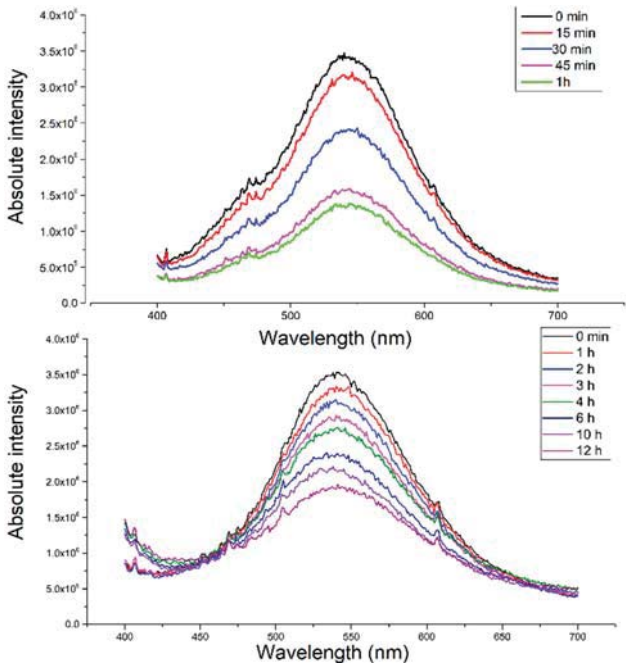

Figure 5. Fluorescence quenching of thin film of **4** deposited on borosilicate glass substrate, detection from gas-phase of (top) 2,4,6-trichloroanisole (TCA), (bottom) trinitrobenzene (TNB).

of 3.026×10^{-5} and 8.47×10^{-9} atm at room temperature, respectively. The lower value for TNB may explain the slower response time for this compound. The maximum concentration of TCA and TNB that can be detected by **4** based on the full value of partial pressure is estimated to be 266 ppb and 74 ppt, respectively. These results demonstrate that **BA**-based CP **4** has excellent sensing ability in the ppb and ppt range. For a test of the reusability of **4** toward vapors of TCA, a substrate coated with **4** was placed in a TCA-saturated environment until complete quenching of **4** was observed. After the substrate was kept under ambient air conditions for 3 h, roughly 80% of the initial emission intensity was recovered (Figure S45).

EXPERIMENTAL SECTION

Materials and Methods. All chemicals were used as received without further purification. **BA** was synthesized using Suzuki cross-coupling reaction of di-9,10-bromoanthracene and 4-pyridine-boronic acid as previously reported.[25]

Fluorescence spectra were measured on a Fluormax-4 and on a Horiba Fluorolog-3 (Jobin Yvon) spectrophotometer. Quantum yield (QY) measurements of solid powder samples were conducted in a Horiba Fluorolog-3 (Jobin Yvon) spectrophotometer equipped with a iHR-320 monochromator and corrected for the instrument response function with integrating sphere setup. Lifetime spectra were collected in the solid state using excitation source 370 nm pulsed LED, photomultiplier R928P obtained from Hamamatsu. Solid-state absorption spectra were collected on a PerkinElmer UV/vis/NIR Lambda 900 (190−1100 nm) instrument and on a Varian Cary 5000 UV/vis/NIR spectrophotometer. IR absorption spectra were recorded on a PerkinElmer FT-IR spectrometer Frontier 4000−400 cm^{-1}. Single crystal diffraction data were obtained from a STOE-IPDS II (single crystal diffractometer λ, Mo Kα radiation, $\lambda = 0.71073$ Å), and the structures were solved and refined using the SHELXT-2014 software package.[54] Thermal analyses (TGA) were performed at a heating rate of 10 °C/min from 20 to 600 °C in a Mettler Toledo SDTA 851a instrument. Powder diffraction XRD investigations were carried out on a STOE STADI P diffractometer with Cu Kα (λ = 1.5406 Å) radiation. Elemental analyses for C, H, and N were carried out using a FLASH 2000 organic elemental analyzer. Mass spectra were performed on a Bruker ION Trap MS and HR-MS instrument with Bruker BioAPEX II. Specific surface measurements, BET, were performed in a Gemini VII surface area analyzer from Micromeritics.

Liquid sensing was performed in a Hellma quartz fluorescent cuvette of 3 mL volume. The sensing experiments of nitro explosives and pesticides were performed in 2.5 mL of acetonitrile (spectroscopic grade) with 1 mg of **4** dispersed in it and with 1 mM concentration of analyte. Spectra were collected on Fluoromax 4 Horiba fluorometer equipped with a stirrer. All experiments were carried out at 375 nm excitation wavelength.

Synthetic Procedures. *{[Zn(μ_2-BA)(MeOH)$_2$(p-Tos)$_2$]}$_n$ (**1**).* Compound **1** was synthesized using Zn(p-Tos)$_2$·xH$_2$O (0.05 mmol) and **BA** (0.1 mmol) in MeOH and DCM solvent mixture ratio 1:1. After stirring for 30 min at room temperature a white precipitate was collected, yield 47% with respect to **BA**.

FT-IR (cm^{-1}): 3409 m, 3069 w, 2915 w, 1617 m, 1542 w, 1495 w, 1215 m, 1185 s, 1124 s, 1076 w, 1037 s, 1007 s, 949 w, 886w, 828 m, 818 m, 771 w, 740 w, 672 s, 642 s, 612 s, 579 s, 504 w. (See the SI, Figure S60.)

Anal. Calcd. for {[Zn(μ_2-BA)(MeOH)$_2$(p-Tos)$_2$]·2DCM}$_n$: C, 51.79; H, 4.35; Cl, 14.56; N, 2.88; O, 13.14; S, 6.58; Zn, 6.70. Found: C, 52.01; H, 4.32; N, 2.82.

For PXRD, calculated powder diffraction fits well with that obtained for bulk material of **1** (see the SI, Figure S51).

*{[Zn(μ_2-BA)(MeOH)$_2$(CF$_3$CO$_2$)$_2$]}$_n$. (**2**).* Compound **2** was synthesized at similar conditions to **1**, but instead of using Zn(p-Tos)$_2$, Zn(CF$_3$CO$_2$)$_2$·xH$_2$O was used. Collected as pale-yellow precipitate, yield 41% based on **BA**.

FT-IR (cm^{-1}): 3089 w, 2975 w, 2853 w, 1658 s, 1603 s, 1542 w, 1448 m, 1415 m, 1389 w, 1188 s, 1133 s, 1067 m, 1000 s, 952 w, 890 w, 833 m, 795 m, 773 m, 746 m, 713 s, 674 m, 639 s, 607 s. (See the SI, Figure S61.)

Anal. Calcd. for {[Zn(μ_2-BA)(MeOH)$_2$(CF$_3$CO$_2$)$_2$]·DCM}$_n$: C, 48.05; H, 3.64; Cl, 9.15; F, 14.71; N, 3.62; O, 12.39; Zn, 8.44. Found: C, 49.41; H, 3.32; N, 3.60.

For PXRD, calculated powder diffraction fits well with that obtained for bulk material of **2** (see the SI, Figure S53).

*{BA@[Zn(μ_2-BA)(MeOH)$_2$(H$_2$O)$_2$](CF$_3$SO$_3$)$_2$}$_n$ (**3**).* Compound **3** was synthesized at similar conditions to **2**, but instead of using Zn(CF$_3$CO$_2$)$_2$, Zn(CF$_3$SO$_3$)$_2$·6H$_2$O was used. Yield is 38% based on **BA**, as fine yellow-green needles after self-diffusion of components over 72 h through the layer of MeOH-DCM.

FT-IR (cm^{-1}): 3066 w, 3022 w, 1593 s, 1533 m, 1517 m, 1483 w, 1444 m, 1394 s, 1318 w, 1252 w, 1217 w, 1186 m, 1147 w, 1060 m, 1031 m, 987 m, 948 w, 882 m, 805 s, 771 s, 727 m, 677 s, 645 s, 610 s. (See the SI, Figure S62.)

Anal. Calcd. for {BA@[Zn(μ_2-BA)(MeOH)$_2$(H$_2$O)$_2$](CF$_3$SO$_3$)$_2$}$_n$: C, 55.40; H, 3.84; F, 10.11; N, 4.97; O, 14.19; S, 5.69; Zn, 5.80. Found: C, 56.82; H, 4.12; N, 5.24.

For PXRD, with complex **3**, unfortunately we were not able to reproduce it in high yield in bulk form; the calculated and obtained diffractogram for bulk did not fit well. Therefore, further analyses were performed in crystalline form, e.g., elemental analysis, fluorescence, UV−vis, except TGA and PXRD, which are not reported here. We expect that TGA of compound **3** would have a similar trend as for complexes **1**, **2**, and **4**.

*{[Cd(μ_2-BA)$_2$(ClO$_4$)$_2$]·n(DCM)}$_n$ (**4**).* Compound **4** was synthesized at similar conditions to compound **2**. Instead of using Zn(CF$_3$CO$_2$)$_2$, Cd(ClO$_4$)$_2$·6H$_2$O was used. Attention: Perchlorates are potentially explosives and should be handled with care! After stirring for 30 min white precipitate was collected, with yield of 78%.

FT-IR (cm^{-1}): 3485 m, 3067 w, 1605s, 1551 w, 1448 w, 1414 m, 1225 m, 1056 b-d, s, 950 w, 920 w, 817 m, 769 m, 741 m, 680 m, 647 s, 605 s. (See the SI, Figure S63.)

Anal. Calcd. for {[Cd(μ_2-BA)$_2$(ClO$_4$)$_2$]}$_n$: C, 52.96; H, 2.96; Cd, 20.65; Cl, 6.51; N, 5.15; O, 11.76. Found: C, 52.24; H, 2.82; N, 5.22.

For PXRD, calculated powder diffraction fits well with that obtained for bulk material of **4** (see the SI, Figure S54).

*{[Cd(μ_2-BA)(MeOH)$_2$(Dioxane)(η_2-SiF$_6$)]·mDioxane}$_n$ (**5**).* Complex **5** was obtained using the synthetic route for **1**. Instead of using Zn(p-Tos)$_2$, CdSiF$_6$·6H$_2$O was used in methanol solution layered over dioxane containing dissolved **BA**; fine plates were obtained after self-diffusion over few days, and yield is 37% based on **BA**.

FT-IR (cm^{-1}): 3412 m, 3068 w, 1603 s, 1538 w, 1440 w, 1418 m, 1397 w, 1221 w, 1071 w, 1020 w, 944 w, 808 w, 775 m, 726 b-d, s, 639 s, 606 s. (See the SI, Figure S64.)

Anal. Calcd. for **5**: C, 37.72; H, 5.91; Cd, 11.77; F, 11.93; N, 2.93; O, 26.80. Found: C, 35.92; H, 5.80; N, 2.98.

For PXRD, calculated powder diffraction well fits with that obtained for bulk material of **5** (see the SI, Figure S55).

Crystallography. X-ray single-crystal diffraction data for **1**−**5** were collected on a STOE IPDS II instrument at 200−250 K with Mo Kα radiation (λ = 0.710 73 Å). The program X-Area[55] was used for the integration of the diffraction profiles. All the structures were solved by dual-space charge flipping method with a SHELXT[56] program of the SHELX package[54] and refined by full-matrix least-squares methods with SHELXL (integration absorption corrections were applied using the X-Red program).[55] Metal atoms in each complex were located from the *E*-maps, and other non-hydrogen atoms were located in successive difference Fourier syntheses and refined with anisotropic thermal parameters on F^2. The hydrogen atoms of the ligands were generated theoretically on the specific atoms and refined *isotropically* with fixed thermal factors. The hydrogen atoms of the solvent molecules were located from Fourier maps and refined with isotropic temperature factors. Highly disordered uncoordinated solvent molecules with site occupancy less than 1 were squeezed by using PLATON software.[57,58] Further details for structural analysis are summarized in Table S9.

Structures can be found by the following CCDC reference numbers **1**, 1843186; **2**, 1843187; **3**, 1843188; **4**, 1843184; **5**, 1843191.

CONCLUSIONS

While generalizations in CP and MOF design should be treated with care, our results suggest that the Zn^{2+}-based CPs obtained using tosylate or trifluoroacetate counterions lead to the formation of 1D structures in which anion−**BA** interactions are important in reducing the separation between the CP chains. Incorporating noncoordinating triflate counterion instead forms 1D structures in which the chains are further apart, generating voids that are filled with an unchelated **BA** guest. Interestingly, a softer and relatively larger cation such as Cd^{2+} forms 2D structures in which the anion participates in the coordination sphere. Thus, double charged SiF_6^{2-} bridges two CP chains similarly to previously reported dicarboxylic acids whereas this is not the case for monovalent perchlorate. This allows for the formation of larger pore sizes, which are suitable for the encapsulation of guests and potential analytes. Coordination polymer **4** was found to possess excellent solution- and vapor-sensing properties toward chloroaromatic herbicide simazine and TCA. Detection of the latter can be used for testing the appearance of cork taint in wines. CP **4** may also have potential applications for the sensing of nitro explosives.

ASSOCIATED CONTENT

Supporting Information

The Supporting Information is available free of charge on the ACS Publications website at DOI: 10.1021/acs.inorgchem.8b03628.

Listing of structure descriptions, UV−vis, solid-state PL, time-resolved measurements, quenching data, PXRD, TGA, IR, BET, and crystallographic data (PDF)

Accession Codes

CCDC 1843184, 1843186−1843188, and 1843191 contain the supplementary crystallographic data for this paper. These data can be obtained free of charge via www.ccdc.cam.ac.uk/data_request/cif, or by emailing data_request@ccdc.cam.ac.uk, or by contacting The Cambridge Crystallographic Data Centre, 12 Union Road, Cambridge CB2 1EZ, UK; fax: +44 1223 336033.

AUTHOR INFORMATION

Corresponding Authors

*E-mail: serhii.vasylevskyi@gmail.com.
*E-mail: katharina.fromm@unifr.ch.

ORCID

Serhii I. Vasylevskyi: 0000-0001-6219-6051
Dario M. Bassani: 0000-0002-9278-1857

Author Contributions

All authors contributed equally.

Funding

Doc. Mobility fellowship P1FRP2_178150 granted by Swiss National Science Foundation SNSF.

Notes

The authors declare no competing financial interest.

ACKNOWLEDGMENTS

We would like to acknowledge the University of Fribourg, the Swiss National Science Foundation SNSF, and the NCCR "Bioinspired Materials" as well as the Fribourg Centre for Nanomaterials FriMat for the support and opportunity to work under this project. We thank Dr. Aurelien Crochet for the help with X-ray diffraction methods and discussions, Dr. Albert Ruggi for HR-MS, and Felix Fehr for NMR measurements. We appreciate support from the Adolphe Merkle Institute (AMI) for providing elemental analysis facilities. S.I.V. acknowledges the SNSF for granting a Doc. Mobility fellowship P1FRP2_178150 to perform part of the work at the University of Bordeaux. Support from ANR Grant ANR-15-JTIC-0001-01 is gratefully acknowledged.

REFERENCES

(1) Xu, H.; Chen, R.; Sun, Q.; Lai, W.; Su, Q.; Huang, W.; Liu, X. Recent Progress in Metal-organic Complexes for Optoelectronic Applications. *Chem. Soc. Rev.* **2014**, *43* (10), 3259−3302.

(2) Huang, J.; Su, J.-H.; Tian, H. The Development of Anthracene Derivatives for Organic Light-Emitting Diodes. *J. Mater. Chem.* **2012**, *22* (22), 10977.

(3) Sun, C.-Y.; Wang, X.-L.; Zhang, X.; Qin, C.; Li, P.; Su, Z.-M.; Zhu, D.-X.; Shan, G.-G.; Shao, K.-Z.; Wu, H.; et al. Efficient and Tunable White-Light Emission of Metal-organic Frameworks by Iridium-Complex Encapsulation. *Nat. Commun.* **2013**, *4*, 2717.

(4) Wu, P.; He, C.; Wang, J.; Peng, X.; Li, X.; An, Y.; Duan, C. Photoactive Chiral Metal-Organic Frameworks for Light-Driven Asymmetric α-Alkylation of Aldehydes. *J. Am. Chem. Soc.* **2012**, *134* (36), 14991−14999.

(5) Chen, D.; Xing, H.; Wang, C.; Su, Z. Highly Efficient Visible-Light-Driven CO $_2$ Reduction to Formate by a New Anthracene-Based Zirconium MOF via Dual Catalytic Routes. *J. Mater. Chem. A* **2016**, *4* (7), 2657−2662.

(6) Gray, V.; Börjesson, K.; Dzebo, D.; Abrahamsson, M.; Albinsson, B.; Moth-Poulsen, K. Porphyrin-Anthracene Complexes: Potential in Triplet-Triplet Annihilation Upconversion. *J. Phys. Chem. C* **2016**, *120* (34), 19018−19026.

(7) Yang, J.; Yue, Q.; Li, G. D.; Cao, J. J.; Li, G. H.; Chen, J. S. Structures, Photoluminescence, up-Conversion, and Magnetism of 2D and 3D Rare-Earth Coordination Polymers with Multicarboxylate Linkages. *Inorg. Chem.* **2006**, *45* (7), 2857−2865.

(8) Quah, H. S.; Chen, W.; Schreyer, M. K.; Yang, H.; Wong, M. W.; Ji, W.; Vittal, J. J. Multiphoton Harvesting Metal-Organic Frameworks. *Nat. Commun.* **2015**, *6* (6), 1−7.

(9) Montalti, M.; Prodi, L.; Zaccheroni, N. Luminescent Chemosensors Based on Anthracene or Dioxyxanthone Derivatives. *J. Fluoresc.* **2000**, *10* (2), 71−71.

(10) Räupke, A.; Palma-Cando, A.; Shkura, E.; Teckhausen, P.; Polywka, A.; Görrn, P.; Scherf, U.; Riedl, T. Highly Sensitive Gas-Phase Explosive Detection by Luminescent Microporous Polymer Networks. *Sci. Rep.* **2016**, *6* (1), 29118.

(11) Gu, T. Y.; Dai, M.; Young, D. J.; Ren, Z. G.; Lang, J. P. Luminescent Zn(II) Coordination Polymers for Highly Selective Sensing of Cr(III) and Cr(VI) in Water. *Inorg. Chem.* **2017**, *56* (8), 4668−4678.

(12) Haldar, R.; Prasad, K.; Samanta, P. K.; Pati, S.; Maji, T. K. Luminescent Metal-Organic Complexes of Pyrene or Anthracene Chromophores: Energy Transfer Assisted Amplified Exciplex Emission and Al^{3+} Sensing. *Cryst. Growth Des.* **2016**, *16* (1), 82−91.

(13) Gong, W.-J.; Ren, Z.-G.; Li, H.-X.; Zhang, J.-G.; Lang, J.-P. Cadmium(II) Coordination Polymers of 4-Pyr-Poly-2-Ene and Carboxylates: Construction, Structure, and Photochemical Double [2 + 2] Cycloaddition and Luminescent Sensing of Nitroaromatics and Mercury(II) Ions. *Cryst. Growth Des.* **2017**, *17* (2), 870−881.

(14) Prasad, K.; Samanta, D.; Haldar, R.; Maji, T. K. Excitation Energy Transfer Supported Amplified Charge-Transfer Emission in an Anthracenedicarboxylate-and Bipyridophenazine- Based Coordination Complex. *Inorg. Chem.* **2018**, *57* (6), 2953−2956.

(15) Chen, J.; Neels, A.; Fromm, K. M. Excimer Formation in Crystalline and Nanostructured Coordination Polymers. *Chem. Commun.* **2009**, *46* (43), 8282.
(16) Chen, J.; Voutier, N.; Rajabi, J.; Crochet, A.; Bassani, D. M.; Fromm, K. M. Influence of Anions and Solvent Molecules on the Packing and Emission Spectra of Coordination Polymers Based on Silver Ions and an Anthracene Derivative. *CrystEngComm* **2017**, *19* (34), 5106−5113.
(17) Anthony, S. P. Organic Solid-State Fluorescence: Strategies for Generating Switchable and Tunable Fluorescent Materials. *ChemPlusChem* **2012**, *77* (7), 518−531.
(18) Shaligram, S.; Wadgaonkar, P. P.; Kharul, U. K. Fluorescent Polymeric Ionic Liquids for the Detection of Nitroaromatic Explosives. *J. Mater. Chem. A* **2014**, *2* (34), 13983.
(19) Vasylevskyi, S. I.; Regeta, K.; Ruggi, A.; Petoud, S.; Piguet, C.; Fromm, K. M. *Cis* - and *Trans* −9,10-Di(1 *H* -Imidazol-1-yl)-Anthracene Based Coordination Polymers of Zn^{II} and Cd^{II}: Synthesis, Crystal Structures and Luminescence Properties. *Dalt. Trans.* **2018**, *47* (2), 596−607.
(20) Shanmugaraju, S.; Mukherjee, P. S. π-Electron Rich Small Molecule Sensors for the Recognition of Nitroaromatics. *Chem. Commun.* **2015**, *51* (89), 16014−16032.
(21) Shanmugaraju, S.; Mukherjee, P. S. Self-Assembled Discrete Molecules for Sensing Nitroaromatics. *Chem. - Eur. J.* **2015**, *21* (18), 6656−6666.
(22) Nagarkar, S. S.; Joarder, B.; Chaudhari, A. K.; Mukherjee, S.; Ghosh, S. K. Highly Selective Detection of Nitro Explosives by a Luminescent Metal-Organic Framework. *Angew. Chem., Int. Ed.* **2013**, *52* (10), 2881−2885.
(23) Li, X.; Yang, L.; Zhao, L.; Wang, X.-L.; Shao, K.-Z.; Su, Z.-M. Luminescent Metal-Organic Frameworks with Anthracene Chromophores: Small-Molecule Sensing and Highly Selective Sensing for Nitro Explosives. *Cryst. Growth Des.* **2016**, *16* (8), 4374−4382.
(24) Biradha, K.; Fujita, M. Coordination Polymers Containing Square Grids of Dimension 15 × 15 Å. *J. Chem. Soc. Dalt. Trans.* **2000**, *0* (21), 3805−3810.
(25) Biradha, K.; Fujita, M. 2D and 1D Coordination Polymers with the Ability for Inclusion of Guest Molecules: Nitrobenzene, Benzene, Alkoxysilanes. *J. Inclusion Phenom. Mol. Recognit. Chem.* **2001**, *41* (1−4), 201−208.
(26) Biradha, K.; Fujita, M. Selective Formation of Rectangular Grid Coordination Polymers with Grid Dimensions 10 × 15, 10 × 20 and 15 × 20. *Chem. Commun.* **2001**, *0* (1), 15−16.
(27) Cui, X.; Khlobystov, A. N.; Chen, X.; Marsh, D. H.; Blake, A. J.; Lewis, W.; Champness, N. R.; Roberts, C. J.; Schröder, M. Dynamic Equilibria in Solvent-Mediated Anion, Cation and Ligand Exchange in Transition-Metal Coordination Polymers: Solid-State Transfer or Recrystallisation? *Chem. - Eur. J.* **2009**, *15* (35), 8861−8873.
(28) Marin, G.; Andruh, M.; Madalan, A. M.; Blake, A. J.; Wilson, C.; Champness, N. R.; Schröder, M. Structural Diversity in Metal-Organic Frameworks Derived from Binuclear Alkoxo-Bridged Copper(II) Nodes and Pyridyl Linkers. *Cryst. Growth Des.* **2008**, *8* (3), 964−975.
(29) Dong, J.-L.; Wang, D.-Z.; Jia, Y.-Y.; Wang, D.-H. hree Coordination Polymers Based on 9,10-Di(Pyridine-4-Yl)Anthracene Ligand: Syntheses, Structures and Fluorescent Properties. *J. Mol. Struct.* **2017**, *1142*, 304−310.
(30) Cui, X.; Khlobystov, A. N.; Chen, X.; Marsh, D. H.; Blake, A. J.; Lewis, W.; Champness, N. R.; Roberts, C. J.; Schröder, M. Dynamic Equilibria in Solvent-Mediated Anion, Cation and Ligand Exchange in Transition-Metal Coordination Polymers: Solid-State Transfer or Recrystallisation? *Chem. - Eur. J.* **2009**, *15* (35), 8861−8873.
(31) We limit the discussion to those systems for which crystals suitable for X-ray crystallographic analysis was possible.
(32) Ou, Y.-C.; Liu, W.-T.; Li, J.-Y.; Zhang, G.-G.; Wang, J.; Tong, M.-L. Solvochromic and Photodimerization Behaviour of 1D Coordination Polymer via Single-Crystal-to-Single-Crystal Transformation. *Chem. Commun.* **2011**, *47* (33), 9384.
(33) Hestand, N. J.; Spano, F. C. Molecular Aggregate Photophysics beyond the Kasha Model: Novel Design Principles for Organic Materials. *Acc. Chem. Res.* **2017**, *50* (2), 341−350.
(34) Würthner, F.; Kaiser, T. E.; Saha-Möller, C. R. j-Aggregates: From Serendipitous Discovery to Supramolecular Engineering of Functional Dye Materials. *Angew. Chem., Int. Ed.* **2011**, *50* (15), 3376−3410.
(35) Sillen, A.; Engelborghs, Y. The Correct Use of "Average" Fluorescence Parameters. *Photochem. Photobiol.* **1998**, *67* (5), 475−486.
(36) Meer, B.; Coker, G.; Chen, S. *Resonance Energy Transfer: Theory and Data*; VCH: Weinheim, 1994.
(37) Hu, Z.; Deibert, B. J.; Li, J. Luminescent Metal-organic Frameworks for Chemical Sensing and Explosive Detection. *Chem. Soc. Rev.* **2014**, *43* (16), 5815−5840.
(38) Lan, A.; Li, K.; Wu, H.; Olson, D. H.; Emge, T. J.; Ki, W.; Hong, M.; Li, J. A Luminescent Microporous Metal-Organic Framework for the Fast Andreversible Detection of High Explosives. *Angew. Chem., Int. Ed.* **2009**, *48* (13), 2334−2338.
(39) Esteve-Núñez, A.; Caballero, A.; Ramos, J. L. Biological Degradation of 2,4,6-Trinitrotoluene. *Microbiol. Mol. Biol. Rev.* **2001**, *65* (3), 335−352.
(40) Buser, H. R.; Zanier, C.; Tanner, H. Identification of 2,4,6-Trichloroanisole as a Potent Compound Causing Cork Taint in Wine. *J. Agric. Food Chem.* **1982**, *30* (2), 359−362.
(41) Tarasov, A.; Rauhut, D.; Jung, R. "Cork Taint" Responsible Compounds. Determination of Haloanisoles and Halophenols in Cork Matrix: A Review. *Talanta* **2017**, *175*, 82−92.
(42) Zhang, J.; Wang, C.; Niu, Y.; Li, S.; Luo, R. Electrochemical Sensor Based on Molecularly Imprinted Composite Membrane of Poly(*o*-aminothiophenol) with Gold Nanoparticles for Sensitive Determination of Herbicide Simazine in Environmental Samples. *Sens. Actuators, B* **2017**, *249*, 747−755.
(43) Ghosh, P.; Paul, S.; Banerjee, P. How Explosive TNP Interacts with a Small Tritopic Receptor: A Combined Crystallographic and Thermodynamic Approach. *CrystEngComm* **2017**, *19* (44), 6703−6710.
(44) Ghosh, P.; Banerjee, P. Small Molecular Probe as Selective Tritopic Sensor of Al^{3+}, F^- and TNP: Fabrication of Portable Prototype for Onsite Detection of Explosive TNP. *Anal. Chim. Acta* **2017**, *965*, 111−122.
(45) Ghosh, P.; Banerjee, P. How Paramagnetic and Diamagnetic LMOCs Detect Picric Acid from Surface Water and the Intracellular Environment: A Combined Experimental and DFT-D3 Study. *Phys. Chem. Chem. Phys.* **2016**, *18* (33), 22805−22815.
(46) Alzaga, R.; Ortiz, L.; Sánchez-Baeza, F.; Marco, M. P.; Bayona, J. M. Accurate Determination of 2,4,6-Trichloroanisole in Wines at Low Parts per Trillion by Solid-Phase Microextraction Followed by GC-ECD. *J. Agric. Food Chem.* **2003**, *51* (12), 3509−3514.
(47) Varelas, V.; Sanvicens, N.; M-Pilar-Marco; Kintzios, S. Development of a Cellular Biosensor for the Detection of 2,4,6-Trichloroanisole (TCA). *Talanta* **2011**, *84* (3), 936−940.
(48) Miller, J. R.; Peeples, J. A.; Schmitt, M. J.; Closs, G. L. Long-Distance Fluorescence Quenching by Electron Transfer in Rigid Solutions. *J. Am. Chem. Soc.* **1982**, *104* (24), 6488−6493.
(49) Inokuti, M.; Hirayama, F. Influence of Energy Transfer by the Exchange Mechanism on Donor Luminescence. *J. Chem. Phys.* **1965**, *43* (6), 1978−1989.
(50) Laferrière, M.; Galian, R. E.; Maurel, V.; Scaiano, J. C. Non-Linear Effects in the Quenching of Fluorescent Quantum Dots by Nitroxyl Free Radicals. *Chem. Commun.* **2006**, *0* (3), 257−259.
(51) The LOD and LOQ were determined from the standard deviation (SD) of a blank sample as LOD = 3SD and LOQ = 10SD.
(52) Joarder, B.; Desai, A. V.; Samanta, P.; Mukherjee, S.; Ghosh, S. K. Selective and Sensitive Aqueous-Phase Detection of 2,4,6-Trinitrophenol (TNP) by an Amine-Functionalized Metal-Organic Framework. *Chem. - Eur. J.* **2015**, *21* (3), 965−969.
(53) Gole, B.; Bar, A. K.; Mukherjee, P. S. Multicomponent Assembly of Fluorescent-Tag Functionalized Ligands in Metal-

Organic Frameworks for Sensing Explosives. *Chem. - Eur. J.* **2014**, *20* (41), 13321−13336.
(54) Sheldrick, G. M. Crystal Structure Refinement with SHELXL. *Acta Crystallogr., Sect. C: Struct. Chem.* **2015**, *71* (1), 3−8.
(55) *X-AREA, X-RED, X-RED32, X-SHAPE*; Stoe & Cie: Darmstadt, Germany, 2002.
(56) Sheldrick, G. M. SHELXT. *Acta Crystallogr., Sect. A: Found. Adv.* **2015**, *71*, 3−8.
(57) Spek, A. L. *Acta Crystallogr., Sect. D: Biol. Crystallogr.* **2009**, *65*, 148−155.
(58) Spek, A. L. PLATON SQUEEZE. *Acta Crystallogr., Sect. C: Struct. Chem.* **2015**, *71*, 9−18.